nature nanotechnology

ARTICLES

PUBLISHED ONLINE: 11 SEPTEMBER 2011 | DOI: 10.1038/NNANO.2011.149

A multifunctional core–shell nanoparticle for dendritic cell-based cancer immunotherapy

Nam-Hyuk Cho[1,2,3†], Taek-Chin Cheong[1,2,4†], Ji Hyun Min[5,6†], Jun Hua Wu[6†], Sang Jin Lee[4], Daehong Kim[4], Jae-Seong Yang[7], Sanguk Kim[7], Young Keun Kim[5,6*] and Seung-Yong Seong[1,2,6*]

Dendritic cell-based cancer immunotherapy requires tumour antigens to be delivered efficiently into dendritic cells and their migration to be monitored *in vivo*. Nanoparticles have been explored as carriers for antigen delivery, but applications have been limited by the toxicity of the solvents used to make nanoparticles, and by the need to use transfection agents to deliver nanoparticles into cells. Here we show that an iron oxide–zinc oxide core–shell nanoparticle can deliver carcinoembryonic antigen into dendritic cells while simultaneously acting as an imaging agent. The nanoparticle–antigen complex is efficiently taken up by dendritic cells within one hour and can be detected *in vitro* by confocal microscopy and *in vivo* by magnetic resonance imaging. Mice immunized with dendritic cells containing the nanoparticle–antigen complex showed enhanced tumour antigen specific T-cell responses, delayed tumour growth and better survival than controls.

Dendritic cells (DCs) are important in the initiation and regulation of antigen-specific immune responses[1] and have been used as potent therapeutic vaccines against human cancers[2–4]. Preliminary results using *ex vivo*-generated DCs that are pulsed with tumour antigens show therapeutic immunity in some cancer patients, but clinical trials have demonstrated poor efficacy[2,5].

To induce DC-based immune responses for destroying tumours, DCs must migrate into the lymph node and activate antigen-specific T cells. The progress of DC migration has been tracked using several non-invasive imaging methods such as scintigraphy[6], single positron emission tomography[7], and magnetic resonance imaging (MRI)[8]. Among these, MRI, which uses superparamagnetic iron oxide (SPIO) nanoparticles, offers exceptional contrast for lymphoid tissues and provides high-resolution *in vivo* images with good signal-to-noise ratios[9]. However, for clinical applications, conventional SPIO nanoparticles must be coated with water-soluble polymers such as dextran to make them biocompatible. Furthermore, cellular uptake of these particles requires a long incubation time (generally >6 h), the use of transfection agents and surface modifications[10–15]. Moreover, because most transfection agents are highly charged, toxic and have a narrow range of non-toxic concentrations, their use needs to be optimized for every clinical setting[11].

Another hurdle in DC-based immunotherapy is the development of a clinically relevant delivery system that can efficiently deliver target antigens into DCs, as sufficient amounts of antigen must be delivered into the DC to generate potent cytotoxic T lymphocytes (CTL) and $CD4^+$ helper T cells, which collaborate to kill tumours[2,16]. Owing to their diverse and unique physicochemical and functional properties, nanoparticles (<100 nm) have been explored for various *in vivo* applications[17,18]. Nanoparticles are good candidates for delivering antigens into DCs because their large surface area allows the immobilization of multiple therapeutic agents[19,20]. Bimodal nanostructures that contain either fluorescent chemicals[21] or quantum dots[22] and SPIO nanoparticles have been used to label DCs for both optical and MRI[23], but their clinical applications are limited by cytotoxicity[24]. To overcome the toxicity issues, disulphonated indocyanine green optical probes together with SPIO nanoparticles were incorporated into poly(lactide-co-glycolide) (PLGA)[23]. When used as a carrier to deliver antigens into DCs, this PLGA-based nanoparticle induced strong CTL responses[25,26]. However, a long incubation period is required for DCs to take up the carrier[23,25] and this method involves emulsifying steps that use organic solvents such as poly(vinyl alcohol) that may affect the antigenicity and stability of loaded antigen[27,28] and the functionality of DCs[29].

Here, we show that multifunctional core–shell nanoparticles consisting of a SPIO core covered with a photonic ZnO shell can be used in DC-based immunotherapy. The nanoparticles were efficiently taken up by DCs without the need for transfection agents and were imaged *in vitro* using a confocal microscope and *in vivo* using MRI. Furthermore, the nanoparticles were designed to have ZnO-binding peptides that could carry tumour antigens (specifically, the carcinoembryonic antigen, CEA[30,31]) into DCs. DCs loaded with the nanoparticle–antigen complex induced anti-tumour immunity *in vivo* and prolonged the survival of immunized mice.

Preparation of Fe_3O_4–ZnO core–shell nanoparticles

The Fe_3O_4–ZnO core–shell nanoparticles were prepared using a modified nanoemulsion method[32]. Nanoparticle synthesis began with the formation of the core (Fe_3O_4) followed by the coating of the shell (ZnO). The manufactured nanoparticles were uniformly spherical and monodispersed (Fig. 1a). Particle size measurements showed that the nanoparticles had an average diameter of 15.7 nm. The increase of 7.2 nm over the ~8.5 nm diameter of the Fe_3O_4 as a result of the surface coating clearly demonstrates the formation of a core–shell nanostructure (Fig. 1a). The

[1]Department of Microbiology and Immunology, [2]Department of Biomedical Sciences, Seoul National University College of Medicine and Institute of Endemic Diseases, Seoul National University Medical Research Center and [3]Bundang Hospital, Seoul, Republic of Korea, [4]Research Institute, National Cancer Center, Goyang, Gyeonggi-do, Republic of Korea, [5]Department of Materials Science and Engineering, Korea University, Seoul, Republic of Korea, [6]Pioneer Research Center for Biomedical Nanocrystals, Korea University, Seoul, Republic of Korea, [7]Department of Life Science and School of Interdisciplinary Bioscience and Bioengineering, Pohang University of Science and Technology, Pohang, Gyungbuk, Republic of Korea; †These authors contributed equally to this work.
*e-mail: seongsy@snu.ac.kr; ykim97@korea.ac.kr

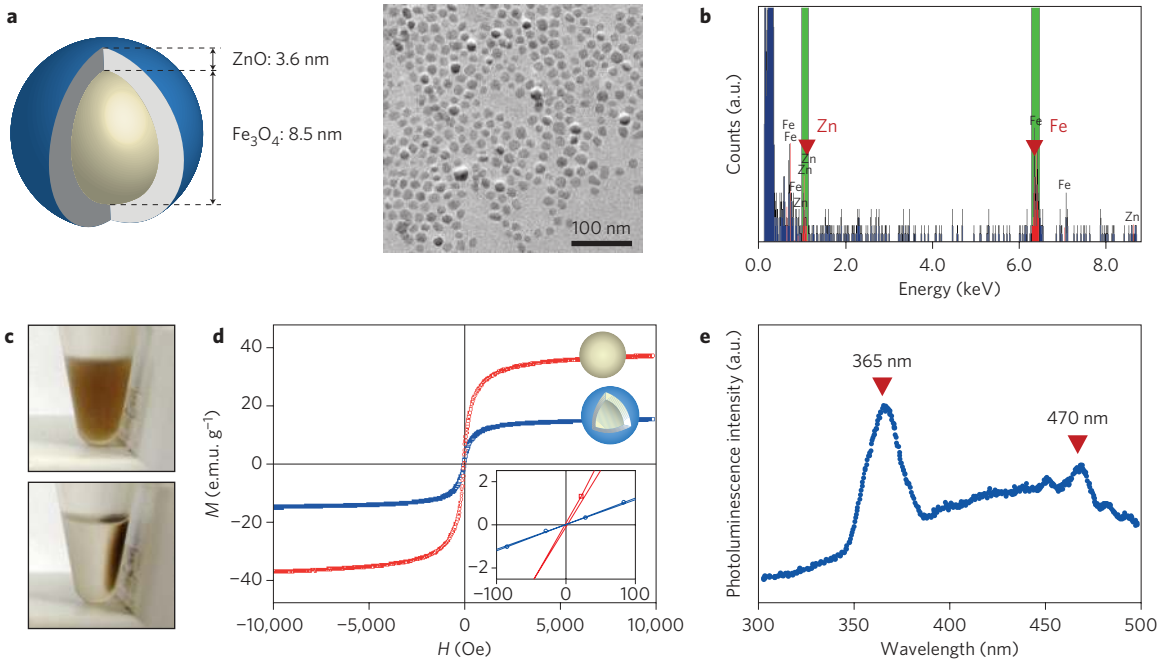

Figure 1 | Characterization of the Fe_3O_4–ZnO core–shell nanoparticle. a, Left: diagram of the core–shell nanoparticle. Right: TEM image of the monodispersed spherical particles. **b**, Point-probe analysis using TEM equipped with EDX, showing that the single nanoparticle consists of both Fe and Zn. **c**, Photographs showing the homogeneous dispersion of nanoparticles (brown) in phosphate-buffered saline (top) and clear transparent solution after collecting the nanoparticles by applying an external magnet (bottom). **d**, Magnetic hysteresis curves of the Fe_3O_4 core part (red) and the Fe_3O_4–ZnO nanoparticles (blue). Inset: details of the hysteresis curves around zero field. **e**, Photoluminescence spectrum of the peptide-linked nanoparticles showing both UV and visible emissions.

composition and nanostructure of the nanoparticles were further confirmed by transmission electron microscopy (TEM) equipped with energy dispersive X-ray spectroscopy (EDX) (Fig. 1b). The point-probe TEM-EDX analysis revealed that a single nanoparticle consists of two compositions of Fe and Zn, corroborating that the ZnO coating process is completed after core formation, and the ZnO composition sits on the surface of the Fe_3O_4 core. The nanoparticles were stable against aggregation after re-dispersion in phosphate buffered saline (Fig. 1c). Under an external magnetic field, the nanoparticles changed from an opaque homogeneous dispersion to a clear and transparent solution within 5 min (Fig. 1c). Magnetic measurements (Fig. 1d) quantitatively revealed well-defined superparamagnetic responses and near-zero coercivity, a property suitable for magnetic actuation and manipulation. As a result of the increase in mass from the addition of non-magnetic ZnO, the saturation magnetization (M_s) of the nanoparticles decreased to 14.7 e.m.u. g^{-1} ('core only' $M_s = 36.7$ e.m.u. g^{-1}), showing the effect of coating.

The ultraviolet-visible spectrum of the nanoparticle exhibited absorption at ~360 nm, as expected for the bandgap excitation of ZnO, and the photoluminescence spectra included the major emission of the ZnO bandgap at ~365 nm as well as additional broad visible emission bands ranging from 370 to 500 nm with peak emission at 470 nm (Fig. 1e), which were related to surface and defect emissions[33–35]. Incorporation of the nanoparticles into DCs increased the mean fluorescent intensity by ~70% compared with the DCs alone when analysed by flow cytometry (excitation at 355 nm and emission at 425–475 nm, Supplementary Fig. S1). Excitation and emission wavelengths above 400 nm are biomedically relevant because of their applicability in fluorescence assays using a flow cytometer or confocal microscope.

To make use of the nanoparticle as an antigen carrier, we genetically fused inorganic-binding peptides to a protein antigen[36]. A novel ZnO-binding peptide (ZBP; amino acid sequence, RPHRKGGDA) was designed based on known peptide sequences showing specific affinity to ZnO[37,38]. This novel peptide consisted of a conserved ZnO-binding motif (RPHRK) and a linker (GGDA) to allow for flexibility (Fig. 2a)[38]. To enhance the binding affinity to ZnO, we further generated a triplicate tandem repeat of the peptide (3 × ZBP). This 3 × ZBP showed enhanced binding to the nanoparticle compared to the 1 × ZBP (Supplementary Fig. S2). The binding of each peptide was saturated when ~1 μg of peptide (equivalent to ~1 nmol for 1 × ZBP and ~0.3 nmol for 3 × ZBP) was used for 100 μg of nanoparticle, resulting in ~3–10 pmol of peptide binding per 1 μg of nanoparticle. When the binding affinity of ZBP to nanoparticle was determined by isothermal titration calorimetry (Fig. 2b,c and Supplementary Table S1), ~3.9 molecules of 1 × ZBP or ~2.3 molecules of 3 × ZBP bound per nanoparticle. As expected, 3 × ZBP ($K_a = 1.4 \times 10^6$ M^{-1}) bound to the nanoparticle approximately twice as strongly as 1 × ZBP ($K_a = 6.9 \times 10^5$ M^{-1}) (Supplementary Table S1). The binding constant of 3 × ZBP is comparable to those of strong inorganic binders with K_a values ranging from 1×10^4 to 1×10^8 M^{-1} (ref. 39). The high affinity of the peptide to the nanoparticle further suggests the presence of Zn ions on the nanoparticle surface.

To generate a complex between a tumour antigen, CEA[30] and nanoparticle, the recombinant 3 × ZBP–CEA fusion protein was incubated with the nanoparticles. Approximately 0.08 μg (~2 pmol) of CEA protein showed saturated binding to 1 μg of nanoparticle, whereas up to 1 μg (~25 pmol) of 3 × ZBP–CEA fusion protein could interact with the same amount of nanoparticle. Therefore, the interaction of the recombinant CEA with 3 × ZBP was enhanced ~12-fold over that of the CEA without 3 × ZBP (Fig. 2d), demonstrating that the tumour antigen could be immobilized efficiently and directly on the nanoparticle when fused with ZBP.

We further investigated the *in vitro* release kinetics of 3 × ZBP from nanoparticles dispersed in cell culture medium containing

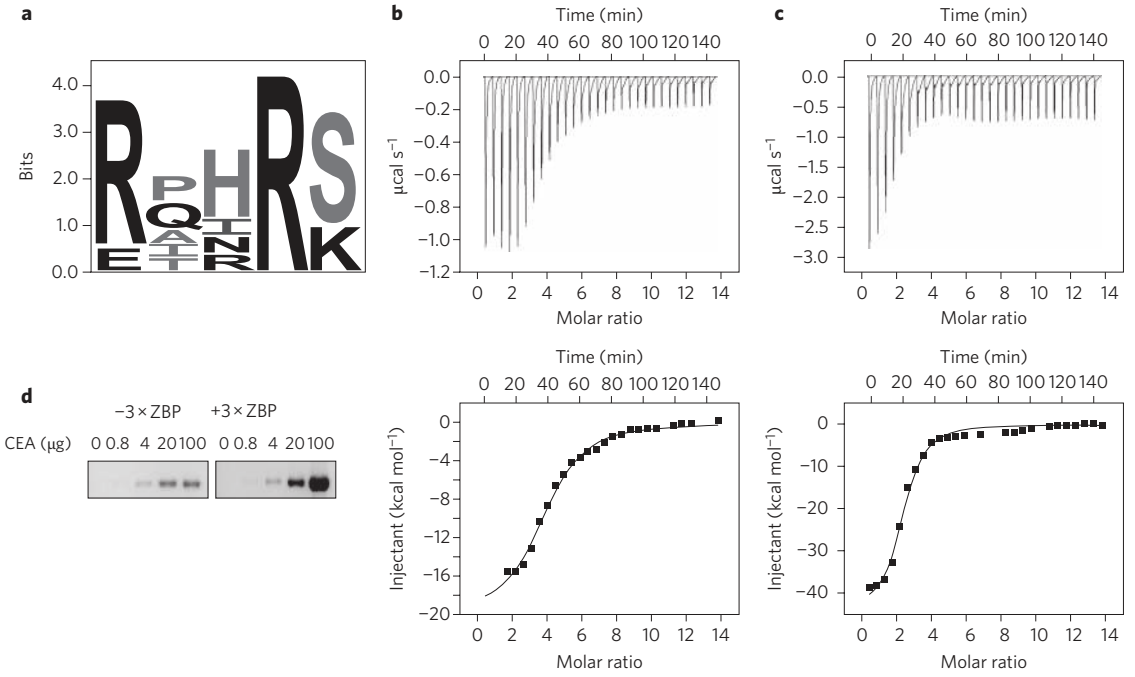

Figure 2 | Immobilization of polypeptide on the nanoparticle. a, Graphical sequence logo representation of ZnO-binding motifs. The conserved sequence pattern was generated using WebLogo3 (http://weblogo.berkeley.edu/). Bits represent the relative frequency of amino acids. **b**,**c**, Detection of the interaction of ZnO-binding peptide (ZBP) with the nanoparticle by isothermal titration calorimetry (ITC). Binding affinity was measured by ITC of 1 × ZBP (**b**) or 3 × ZBP (**c**) (0.25 mM each) with a solution of nanoparticle (4 μM). The ITC raw data (top) and the integrated heat data (bottom), corrected for dilution, are shown. **d**, Gel electrophoresis data showing nanoparticle-bound CEA after incubation with nanoparticles (50 μg) and the indicated amounts of CEA with or without 3 × ZBP fusion. Bound CEA was resolved by sodium dodecyl sulphate polyacrylamide gel electrophoresis after extensive washing of nanoparticles.

10% fetal bovine serum (FBS). The peptides bound to nanoparticles stably associated with nanoparticles in culture medium for the first 4 h of incubation and gradually released thereafter (Supplementary Fig. S3). After 12 h of incubation, half of the bound peptides were dissociated from the nanoparticles, and were not detectable by day 3. The 1 × ZBP demonstrated similar *in vitro* release kinetics (Supplementary Fig. S3). The stable association of the peptides with nanoparticles for up to 4 h in cell culture medium may enhance antigen delivery into DCs without losing them into the medium, and the continuous release of antigen within cells can promote antigen processing and presentation by DCs.

Delivery of core–shell nanoparticles into DCs

Phagocytic immature DCs were incubated with 100 μg ml^{-1} Fe_3O_4 of nanoparticles or Fe_3O_4–ZnO nanoparticles for different durations (Fig. 3a,b). Interestingly, the Fe_3O_4–ZnO nanoparticles were taken up by the DCs much more efficiently than the Fe_3O_4 nanoparticles for the first 8 h, although there was no significant difference after 20 h of incubation. More than 95% of DCs took up substantial amounts of Fe_3O_4–ZnO nanoparticles after 1 h of incubation (Fig. 3a), which is comparable to a former report for ZnO nanoparticles[40]. This suggests that the ZnO shell could facilitate the intracellular delivery of nanoparticles and reduce the incubation time for labelling DCs. More than 95% of DCs took up substantial amounts of Fe_3O_4–ZnO nanoparticles after 1 h of incubation (Fig. 3a), which is comparable to a former report for ZnO nanoparticles[40]. Considering that the labelling of DCs with conventional Fe_3O_4 nanoparticles requires an enhancing agent[41] such as protamine sulphate[42] or long incubation periods (typically 16–48 h)[8,9,43], the core–shell nanoparticles are far better than conventional Fe_3O_4 nanoparticles in that they require only 1 h incubation and no transfection agents or surface modification.

Photoluminescence of the ZnO[44] allowed the nanoparticles to be examined using confocal microscopy after delivery into the DC cytosol (Fig. 3c and Supplementary Fig. S4). When the nanoparticle-labelled DCs were excited at a wavelength of 405 nm, the cells showed higher fluorescent intensity at broad emission wavelengths ranging from 465 to 679 nm. However, the peak emission was observed at 529–550 nm, which can be easily detected by a conventional flow cytometer or confocal microscope (Supplementary Fig. S4). The nanoparticles dispersed throughout the cytoplasm and were found in aggregated forms (Fig. 3c), which might have been taken up by phagocytosis[19]. 3 × ZBP immobilized on the nanoparticles was also efficiently delivered into the cytoplasm of DCs (Fig. 3d), and formed peptide aggregates that partially co-localized with endosomes or lysosomes (Fig. 3d), indicating the peptide–nanoparticle complexes were internalized through phagocytosis[19]. When 3 × ZBP–CEA nanoparticle complexes were incubated with the cells, the mean fluorescence intensity, representing the intracellular contents of CEA, increased by a factor of ~6 compared to that of CEA alone (Fig. 3e). This suggests that immobilization of CEA onto core–shell nanoparticles using 3 × ZBP can facilitate intracellular uptake of tumour antigen by DCs.

To evaluate the cellular toxicity of the nanoparticles, we incubated DCs with different amounts of nanoparticles (12.5–400 μg ml^{-1}) for 3 days or with 100 μg ml^{-1} nanoparticles for 1 to 7 days, and observed no significant changes in viability (Supplementary Fig. S5). In addition, the surface expression of the maturation markers (MHC II, CD40, CD80 and CD86) on the DCs was not significantly affected by the nanoparticle loading (Supplementary Fig. S6). The antigen-capturing and processing capacity of DCs irreversibly reduces as they mature[45]. Therefore, rapid and efficient antigen uptake without DC maturation followed by DC activation using lipopolysaccahride (LPS) or cytokine cocktails might facilitate efficient antigen presentation after DC maturation, which

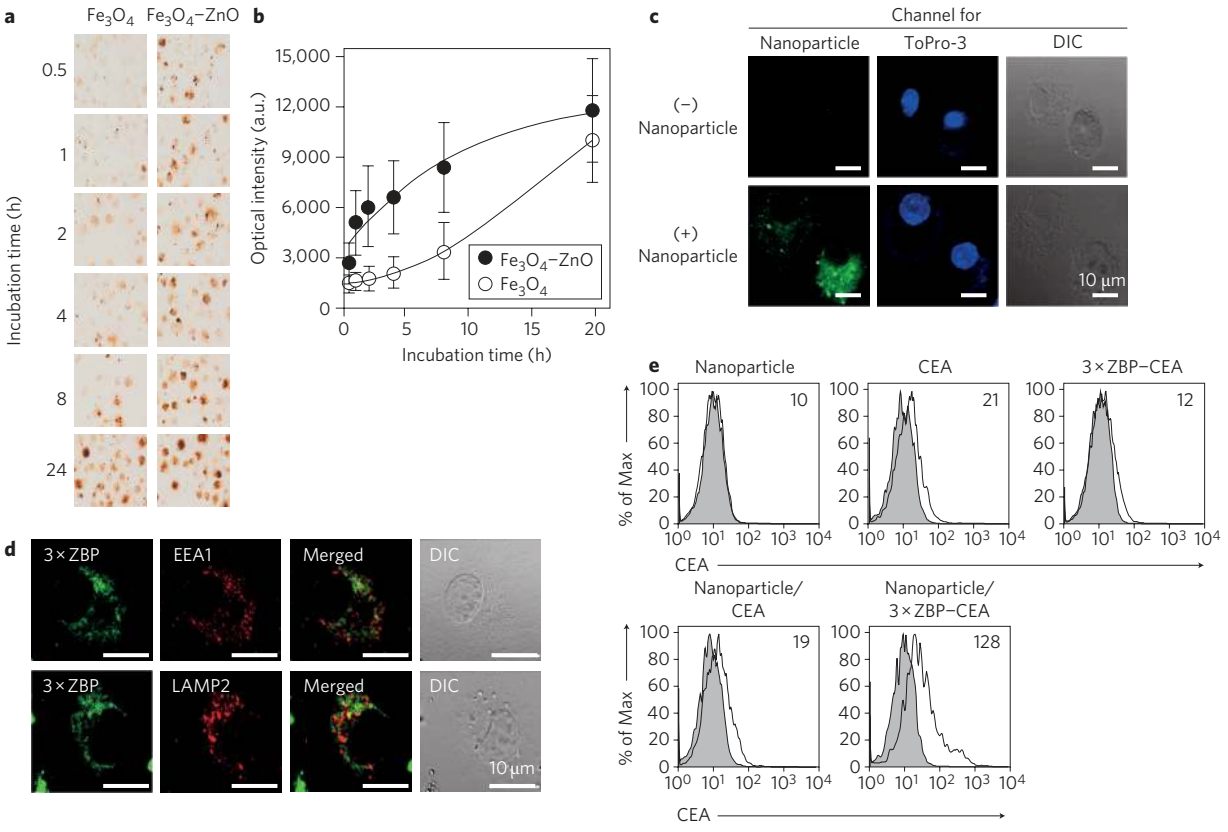

Figure 3 | Intracellular delivery of the nanoparticles into DCs. a, Intracellular nanoparticles visualized by DAB-enhanced Prussian blue staining of DCs labelled with 100 μg ml^{-1} of Fe_3O_4 nanoparticles or Fe_3O_4–ZnO nanoparticles after incubation for the indicated time. **b**, Optical intensities of 100 randomly selected cells from each sample in **a**. Error bars, standard error of the mean. **c**, Fluorescence images of DCs loaded without (top) or with (bottom) nanoparticles (green). Nuclei (blue) were stained with ToPro-3. DIC, differential interference contrast. **d**, Fluorescence images of DCs incubated with nanoparticle–3 × ZBP complexes. Intracellular 3 × ZBP (green) was stained together with EEA1 (endosomes) or LAMP2 (lysosomes). **e**, Flow cytometric analysis of DCs incubated with nanoparticle-recombinant CEA complexes. The mean fluorescence intensities of intracellular CEA (line) were shown within the histograms. Grey histogram, isotype control.

may eventually enhance the immune response against the loaded antigen.

Detection of nanoparticle-labelled DCs by MRI

DCs were incubated with different amounts of nanoparticles (0–160 μg ml^{-1}) to determine the optimal concentration for MRI (Fig. 4a). MRI of the DCs *in vitro* revealed that the T2 relaxation time reduced gradually (image was darkened), with maximal saturation at 160 μg ml^{-1} (Fig. 4a). To define the optimal incubation time, DCs were cultured in the presence 40 μg ml^{-1} of the nanoparticles for 0.5–4 h. The DCs were saturated with the nanoparticles within 1 h (Fig. 4b), indicating that the nanoparticles were efficiently taken up by the DCs within this period, as observed in the experiment using Prussian blue (Fig. 3a), and showed a sufficient reduction of T2 relaxation time under MRI. As expected, MRI of the core–shell nanoparticle-labelled cells showed a more rapid reduction in T2 relaxation time in the first 4 h than for the Fe_3O_4-labelled DCs (Fig. 4b). These results indicate that labelling 1×10^6 DCs with 40 μg ml^{-1} of nanoparticle for 1 h provided sufficient signal reduction in MRI.

Nanoparticle-labelled cells were injected into the hind footpads of C57BL/6 mice to monitor DC trafficking by MRI *in vivo*. The popliteal lymph nodes were monitored for signs of DC migration from the injected footpads using a T2-weighted multigradient echo MR sequence. At 48 h after injection, localized hypointense regions within the left lymph nodes were identified, indicating the presence of the nanoparticle-labelled cells (Fig. 4c, left panel, red arrow). As expected, T2 reduction was not observed in the popliteal lymph nodes corresponding to the injection sites of DCs labelled with ZnO nanoparticles (Fig. 4c, left panel, yellow arrow). The nanoparticle-labelled DCs were observed in the central parts of the draining lymph nodes, indicating that the T2 reduction was due to the nanoparticle-labelled DCs, rather than free nanoparticles transported via the lymphatic vessels. The free nanoparticles were generally localized at the subcapsular region of the lymph node after being transported through lymphatic vessels[42,46]. When cell-free nanoparticles (500 μg) were injected directly into the footpads, we could not observe any significant signal reduction in the draining lymph node (Fig. 4c, right panel, green arrow). A combination of 3,3′-diaminobenzidine (DAB)-enhanced Prussian blue staining and immunohistochemistry of the dissected lymph node revealed that nanoparticle-labelled DCs were mostly within the central Thy1.2$^+$ T-cell areas but not in the B220$^+$ B-cell follicles (anti-Thy1.2, upper panel of Fig. 4d; anti-B220, lower panel). In contrast, no iron was detected in the control lymph nodes corresponding to the injection sites of DCs labelled with ZnO nanoparticles (data not shown). These results clearly indicate that migratory DCs loaded with nanoparticles, and not passive transport of nanoparticles, is responsible for the signal reduction in the central T-cell zone of draining lymph nodes observed by MRI.

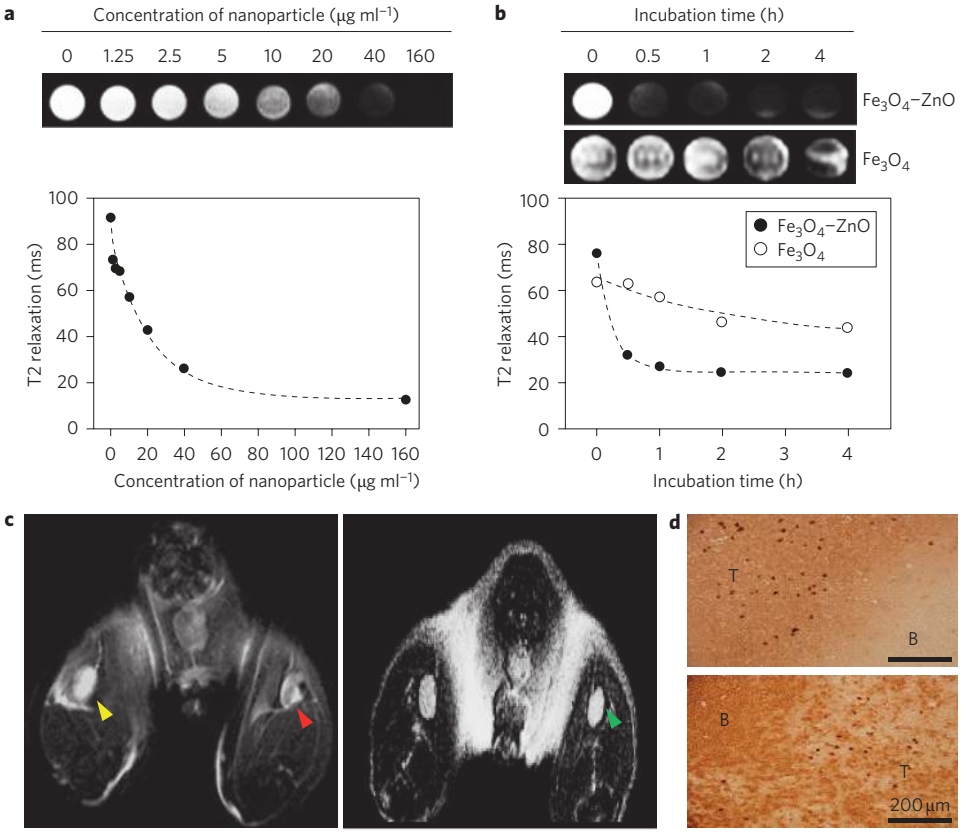

Figure 4 | *In vitro* and *in vivo* MRI of nanoparticle-labelled DCs. a, *In vitro* MRI image (top) of DCs labelled with different amounts of Fe_3O_4–ZnO nanoparticles for 1 h and T2 relaxation time plot (bottom). **b**, *In vitro* MRI images (top) and T2 relaxation time plot (bottom) of DCs incubated with 40 μg ml^{-1} Fe_3O_4–ZnO or Fe_3O_4 nanoparticles for the indicated time. **c**, *In vivo* MRI images of draining lymph nodes of a mouse (left) injected with DCs labelled with Fe_3O_4–ZnO (red arrow) or ZnO nanoparticles (yellow arrow) into the ipsilateral footpads. Right shows a draining lymph node (green arrow) of cell-free Fe_3O_4–ZnO nanoparticle-injected mouse. **d**, Representative immunohistochemistry of draining lymph node after injection with Fe_3O_4-ZnO nanoparticle-labelled DCs (dark brown dots). T, T-cell zone (Thy1.2$^+$), B, B-cell follicle (B220$^+$).

Nanoparticle-labelled DCs induce anti-tumour immunity

To investigate whether the present nanoparticles can be used in DC-based cancer immunotherapy, we immunized C57BL/6 mice with DCs loaded with the nanoparticle–CEA complex and analysed CEA-specific cellular immunity. Lymphocytes from mice immunized with DC(nanoparticle/3 × ZBP–CEA) exhibited greater dose-dependent proliferation in response to CEA than those from the control groups (Fig. 5a). Prominent cytotoxic responses against CEA-expressing cancer cells (MC38/CEA) were induced in mice immunized with DC(nanoparticle/3 × ZBP–CEA), whereas no significant cytotoxicity was detected in the control groups (Fig. 5b, right panel). The cytotoxicity of splenocytes against CEA-negative MC38 target cells was not significant in any of the experimental groups (Fig. 5b, left panel), suggesting that the cytotoxic responses were specific to CEA.

We next examined T-cell responses by measuring their production of IFN-γ, a hallmark cytokine for cell-mediated immunity, in an antigen-dependent manner (Fig. 5c). The frequency of IFN-γ-secreting CD8$^+$ T cells in spleen increased approximately tenfold in mice immunized with DC(nanoparticle/3 × ZBP–CEA). In contrast, spleen CD8$^+$ T cells from other control groups did not show significant IFN-γ secretion after antigenic stimulation. The DC(nanoparticle/3 × ZBP–CEA) group was also more effective at generating CEA-specific, IFN-γ-producing CD4$^+$ or CD8$^+$ T cells in the draining lymph nodes than the other DC groups (Supplementary Fig. S7). These results show that DC(nanoparticle/3 × ZBP–CEA) can efficiently generate CEA-specific cellular immunity *in vivo*.

Compared with the control groups, tumour growth was significantly suppressed in mice immunized with DC(nanoparticle/3 × ZBP–CEA) (Fig. 6a, left panel). At day 40 following tumour inoculation, all five mice treated with DC(nanoparticle/3 × ZBP–CEA) survived, whereas the mice in all other groups died (Fig. 6a, right panel). The mean survival period of mice immunized with DC(nanoparticle/3 × ZBP–CEA) was extended to 19.5 days from 10.5 days for the control groups. The delayed tumour growth and prolonged survival of tumour-bearing mice correlated with the efficiency of intracellular delivery of the tumour antigen into DCs (Fig. 3e). The therapeutic outcomes of this study were comparable to those of our previous work using a protein-transduction domain, Tat, as a CEA antigen delivery tool[4], suggesting that the current nanoparticle-based system is as efficient as the conventional protein transduction system. The anti-tumour immunity of this DC formulation was further validated using a transgenic mouse spontaneously expressing human CEA (Fig. 6b). CEA-transgenic mice are tolerant to this self-antigen and therefore provide a potential preclinical model to assess the induction of anti-CEA immune responses[31,47]. When the transgenic mice were immunized with DC(nanoparticle/3 × ZBP–CEA), tumour growth was significantly suppressed compared to the control groups (Fig. 6b). This strongly suggests that DCs pulsed with nanoparticle/3 × ZBP–CEA can

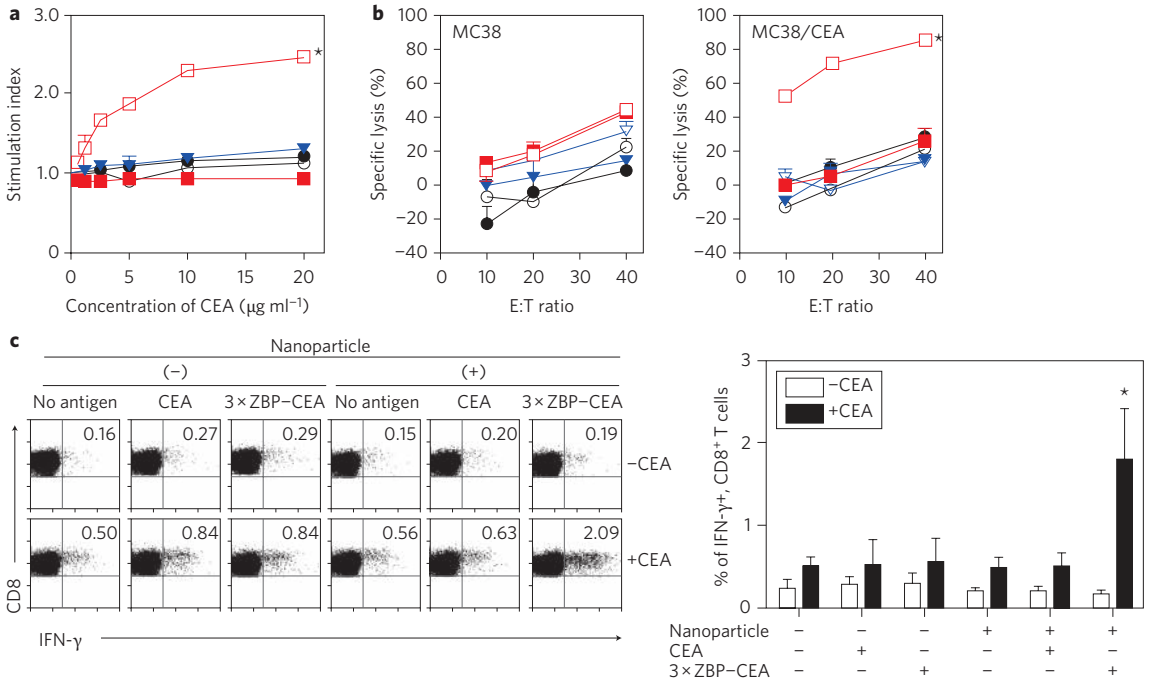

Figure 5 | Induction of CEA-specific immunity. a, *In vitro* proliferation of lymphocytes from immunized mice after CEA stimulation. Mice were immunized with DCs loaded with nanoparticle/3 × ZBP–CEA (open red squares), nanoparticle/CEA (filled red squares), 3 × ZBP–CEA (open blue triangles), CEA (filled blue triangles), nanoparticle (open black circles) or DC only (filled black circles). Error bars, standard error of three independent experiments. **b**, CEA-specific cytotoxic activity of splenocytes from immunized mice. MC38 cells with (MC38/CEA) or without (MC38) CEA expression were used as targets. Symbols as in **a**. **c**, CEA-specific, IFN-γ^+ $CD8^+$ T-cell responses of mice immunized with DCs as in **a**. IFN-γ^+ CTLs in splenocytes were detected in the presence (+) or absence (–) of CEA. Left panel: representative dot plots. Right panel: average percentiles of the CTL from three independent experiments. *$P < 0.05$ by Student's *t*-test.

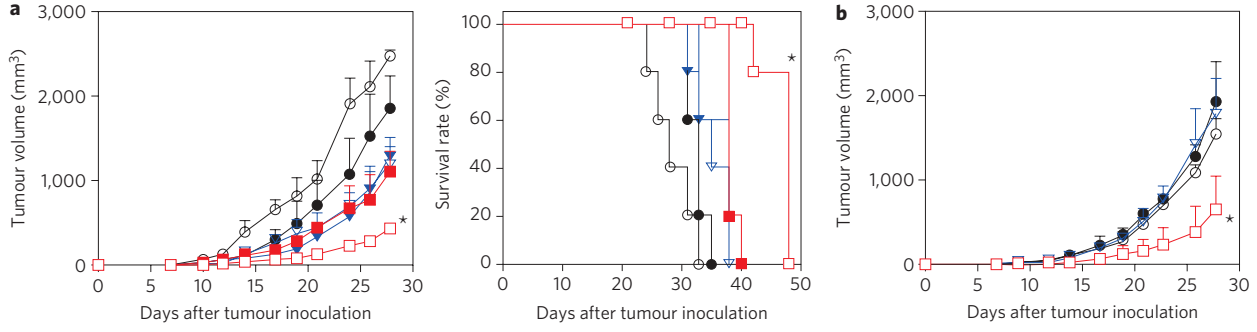

Figure 6 | Tumour growth and survival of immunized mice. a, Tumour volume (left) and survival rate (right) of mice (5 mice/group) injected with MC38/CEA cells. Mice were immunized with DCs, loaded with nanoparticle/3 × ZBP–CEA (open red squares), nanoparticle/CEA (filled red squares), 3 × ZBP–CEA (open blue triangles), CEA (filled blue triangles), nanoparticle (open black circles) or DC only (filled black circles), four times at weekly intervals starting one week after tumour injection. **b**, Tumour growth in human CEA-transgenic mice (5 mice/group) inoculated with MC38/CEA cells. Mice were immunized with DCs three times at weekly intervals and the symbols are the same as in **a**. Error bars, standard error of the mean. *$P < 0.05$ by Student's *t*-test for tumour volumes and $P < 0.01$ using the Kaplan–Meier method (log-rank test).

break peripheral T-cell tolerance against CEA and induce potent protective immune responses against CEA-positive tumours *in vivo*.

Conclusions

In this study, we demonstrated cancer immunotherapy using DCs pulsed with multifunctional core–shell nanoparticles consisting of a superparamagnetic Fe_3O_4 core covered with a photonic ZnO shell. The nanoparticles provided simple and consistent outcomes for the *ex vivo* antigen loading of DCs, for *in vivo* tracking and induction of strong anti-CEA immune responses, even in an immune-tolerant host. The ability of the nanoparticles to be efficiently loaded into DCs in a short incubation period (~1 h) without surface modifications or transfection agents may expedite clinical trials. It might be possible to bypass the complex chemical modifications of the Fe_3O_4 surface that are generally performed in an organic environment to conjugate tumour antigens, a step that has the potential to alter their antigenicity. When combined with a tumour-associated antigen, nanoparticle-loaded DCs did not show changes in viability and phenotype. Taken together, the core–shell nanoparticle could be applied in diverse DC-based immunotherapies that need to monitor antigen loading *in vitro* and track DCs *in vivo* to ensure consistent clinical efficacy.

Methods

Synthesis and characterization of Fe_3O_4–ZnO core–shell nanoparticles. The Fe_3O_4–ZnO nanoparticles were prepared using a modified nanoemulsion method[32]. The Fe_3O_4 core was generated by reduction of iron(III) acetylacetonate ($Fe(acac)_3$, 99.9%, Aldrich) in octyl ether ($C_8H_{17}OC_8H_{17}$, 99%, Wako) in the presence of poly(ethylene glycol)-block-poly(propylene glycol)-block-poly(ethylene glycol) (PEO-PPO-PEO, Aldrich) and 1,2-hexadecandiol ($C_{14}H_{29}CH(OH)CH_2(OH)$, 90%, Aldrich). The solution was homogenized at a high temperature (300 °C) under vigorous stirring for nucleation and formation of the Fe_3O_4 nanoparticles. After cooling to room temperature, zinc acetylacetonate ($Zn(acac)_2$, 99.9%, Aldrich) and 1,2-hexadecanediol were added to the solution to coat the ZnO shells. The reaction profile was started by heating the solution, homogenizing it, rapidly heating to 300 °C, and refluxing at the same temperature. Ethanol was then added to the product mixture to precipitate the nanoparticles, which were purified several times and separated by centrifugation.

The morphology, composition and nanostructure of the nanoparticles were measured by TEM (JEOL 2010F) equipped with EDX. To prepare the samples for TEM measurement, nanoparticles dispersed in hexane were dropped onto carbon-supported copper grids. A vibrating sample magnetometer (Lakeshore 7300) was used to perform magnetic measurements. The optical properties of the nanoparticles were investigated by ultraviolet-visible spectroscopy (Agilent 8453E) and spectrofluorophotometry (Shimadzu RF-5301PC).

Design and preparation of ZnO-binding peptide. To design the ZBP, sequences of high-affinity ZnO binding patterns were collected from the referenced studies[37,38]. Clustering of the high-affinity binding peptides revealed the existence of the motif. A sequence logo was applied to find the most frequent sequence pattern[48]. Graphical representation of the sequence logo indicated the Zn binding motifs RPHRS and RPHRK (Fig. 2a). High-affinity ZBP frequently contains the RXXRK motif[38], suggesting its important role in ZnO binding. In addition, tandem repeats of the ZnO binding motif were considered for the design of ZBP to increase its chance of interaction. Flexible linker residues (GGDA) were inserted between the RPHRK motifs to increase the flexibility of the neighbouring ZnO binding motifs and to permit peptide binding without steric hindrance. *N*-terminal biotinylated ZBP peptides (>90% purity) were synthesized using a peptide synthesizer (PeptrEXTM, Peptron) and then analysed by mass spectrometry and high-performance liquid chromatography using C-18 column chromatography.

Received 3 May 2011; accepted 4 August 2011;
published online 11 September 2011

References

1. Seong, S. Y. & Matzinger, P. Hydrophobicity: an ancient damage-associated molecular pattern that initiates innate immune responses. *Nature Rev. Immunol.* **4,** 469–478 (2004).
2. Palucka, A. K., Ueno, H., Fay, J. W. & Banchereau, J. Taming cancer by inducing immunity via dendritic cells. *Immunol. Rev.* **220,** 129–150 (2007).
3. Melief, C. J. Cancer immunotherapy by dendritic cells. *Immunity* **29,** 372–383 (2008).
4. Bae, M. Y., Cho, N. H. & Seong, S. Y. Protective anti-tumour immune responses by murine dendritic cells pulsed with recombinant Tat-carcinoembryonic antigen derived from *Escherichia coli*. *Clin. Exp. Immunol.* **157,** 128–138 (2009).
5. Figdor, C. G., de Vries, I. J., Lesterhuis, W. J. & Melief, C. J. Dendritic cell immunotherapy: mapping the way. *Nature Med.* **10,** 475–480 (2004).
6. De Vries, I. J. *et al.* Effective migration of antigen-pulsed dendritic cells to lymph nodes in melanoma patients is determined by their maturation state. *Cancer Res.* **63,** 12–17 (2003).
7. Prince, H. M. *et al. In vivo* tracking of dendritic cells in patients with multiple myeloma. *J. Immunother.* **31,** 166–179 (2008).
8. de Vries, I. J. *et al.* Magnetic resonance tracking of dendritic cells in melanoma patients for monitoring of cellular therapy. *Nature Biotechnol.* **23,** 1407–1413 (2005).
9. Dekaban, G. A. *et al.* Semiquantitation of mouse dendritic cell migration *in vivo* using cellular MRI. *J. Immunother.* **32,** 240–251 (2009).
10. Bulte, J. W. *In vivo* MRI cell tracking: clinical studies. *Am. J. Roentgenol.* **193,** 314–325 (2009).
11. Rogers, W. J., Meyer, C. H. & Kramer, C. M. Technology insight: *in vivo* cell tracking by use of MRI. *Nature Clin. Practice* **3,** 554–562 (2006).
12. Martin, A. L., Bernas, L. M., Rutt, B. K., Foster, P. J. & Gillies, E. R. Enhanced cell uptake of superparamagnetic iron oxide nanoparticles functionalized with dendritic guanidines. *Bioconjug. Chem.* **19,** 2375–2384 (2008).
13. Sun, R. *et al.* Physical and biological characterization of superparamagnetic iron oxide- and ultrasmall superparamagnetic iron oxide-labeled cells: a comparison. *Invest. Radiol.* **40,** 504–513 (2005).
14. Kunzmann, A. *et al.* Efficient internalization of silica-coated iron oxide nanoparticles of different sizes by primary human macrophages and dendritic cells. *Toxicol. Appl. Pharmacol.* **253,** 81–93 (2011).
15. Chen, C. L. *et al.* A new nano-sized iron oxide particle with high sensitivity for cellular magnetic resonance imaging. *Mol. Imag. Biol.* http://dx.doi.org/10.1007/s11307-010-0430-x (2010).
16. Gilboa, E. DC-based cancer vaccines. *J. Clin. Invest.* **117,** 1195–1203 (2007).
17. Nel, A. E. *et al.* Understanding biophysicochemical interactions at the nano–bio interface. *Nature Mater.* **8,** 543–557 (2009).
18. Sanvicens, N. & Marco, M. P. Multifunctional nanoparticles—properties and prospects for their use in human medicine. *Trends Biotechnol.* **26,** 425–433 (2008).
19. Sun, C., Lee, J. S. & Zhang, M. Magnetic nanoparticles in MR imaging and drug delivery. *Adv. Drug Deliv. Rev.* **60,** 1252–1265 (2008).
20. Klippstein, R. & Pozo, D. Nanotechnology-based manipulation of dendritic cells for enhanced immunotherapy strategies. *Nanomedicine* **6,** 523–529 (2010).
21. Cruz, L. J. *et al.* Multimodal imaging of nanovaccine carriers targeted to human dendritic cells. *Mol. Pharm.* **8,** 520–531 (2011).
22. Mackay, P. S. *et al.* Multimodal imaging of dendritic cells using a novel hybrid magneto-optical nanoprobe. *Nanomedicine* **7,** 489–496 (2011).
23. Lim, Y. T. *et al.* Biocompatible polymer-nanoparticle-based bimodal imaging contrast agents for the labeling and tracking of dendritic cells. *Small* **4,** 1640–1645 (2008).
24. Chang, E., Thekkek, N., Yu, W. W., Colvin, V. L. & Drezek, R. Evaluation of quantum dot cytotoxicity based on intracellular uptake. *Small* **2,** 1412–1417 (2006).
25. Zhang, Z. *et al.* Induction of anti-tumor cytotoxic T cell responses through PLGA-nanoparticle mediated antigen delivery. *Biomaterials* **32,** 3666–3678 (2011).
26. Noh, Y. W., Jang, Y. S., Ahn, K. J., Lim, Y. T. & Chung, B. H. Simultaneous *in vivo* tracking of dendritic cells and priming of an antigen-specific immune response. *Biomaterials* **32,** 6254–6263 (2011).
27. Bilati, U., Allemann, E. & Doelker, E. Nanoprecipitation versus emulsion-based techniques for the encapsulation of proteins into biodegradable nanoparticles and process-related stability issues. *AAPS PharmSciTech* **6,** E594–E604 (2005).
28. Stivaktakis, N. *et al.* PLA and PLGA microspheres of beta-galactosidase: effect of formulation factors on protein antigenicity and immunogenicity. *J. Biomed. Mater. Res. A* **70,** 139–148 (2004).
29. Blank, F. *et al.* Biomedical nanoparticles modulate specific CD4(+) T cell stimulation by inhibition of antigen processing in dendritic cells. *Nanotoxicology* http://dx.doi.org/10.3109/17435390.2010.5141293 (2011).
30. Wang, D., Rayani, S. & Marshall, J. L. Carcinoembryonic antigen as a vaccine target. *Exp. Rev. Vaccines* **7,** 987–993 (2008).
31. Bhattacharya-Chatterjee, M., Saha, A., Foon, K. A. & Chatterjee, S. K. Carcinoembryonic antigen transgenic mouse models for immunotherapy and development of cancer vaccines. *Curr. Protoc. Immunol.* **20,** Unit 20 28 (2008).
32. Liu, H. L., Sonn, C. H., Wu, J. H., Lee, K. M. & Kim, Y. K. Synthesis of streptavidin-FITC-conjugated core–shell Fe_3O_4–Au nanocrystals and their application for the purification of $CD4^+$ lymphocytes. *Biomaterials* **29,** 4003–4011 (2008).
33. Millers, D., Grigorjeva, L., Lojkowski, W. & Strachowski, T. Luminescence of ZnO nanopowders. *Radiat. Meas.* **38,** 589–591 (2004).
34. Wu, Y. L., Tok, A. I. Y., Boey, F. Y. C., Zeng, X. T. & Zhang, X. H. Chemical synthesis of ZnO nanocrystals. *IEEE Trans. Nanotechnol.* **6,** 497–503 (2006).
35. Dong, L. *et al.* Preparation of ZnO colloids by aggregation of the nanocrystal subunits. *J. Colloid Interface Sci.* **283,** 380–384 (2005).
36. Sarikaya, M., Tamerler, C., Schwartz, D. T. & Baneyx, F. O. Materials assembly and formation using engineered polypeptides. *Annu. Rev. Mater. Res.* **34,** 373–408 (2004).
37. Kjaergaard, K., Sorensen, J. K., Schembri, M. A. & Klemm, P. Sequestration of zinc oxide by fimbrial designer chelators. *Appl. Environ. Microbiol.* **66,** 10–14 (2000).
38. Thai, C. K. *et al.* Identification and characterization of Cu(2)O- and ZnO-binding polypeptides by *Escherichia coli* cell surface display: toward an understanding of metal oxide binding. *Biotechnol. Bioeng.* **87,** 129–137 (2004).
39. Seker, U. O. & Demir, H. V. Material binding peptides for nanotechnology. *Molecules* **16,** 1426–1451 (2011).
40. Xia, T. *et al.* Comparison of the mechanism of toxicity of zinc oxide and cerium oxide nanoparticles based on dissolution and oxidative stress properties. *ACS Nano* **2,** 2121–2134 (2008).
41. Mailander, V. & Landfester, K. Interaction of nanoparticles with cells. *Biomacromolecules* **10,** 2379–2400 (2009).
42. Baumjohann, D. *et al. In vivo* magnetic resonance imaging of dendritic cell migration into the draining lymph nodes of mice. *Eur. J. Immunol.* **36,** 2544–2555 (2006).
43. Raynal, I. *et al.* Macrophage endocytosis of superparamagnetic iron oxide nanoparticles: mechanisms and comparison of ferumoxides and ferumoxtran-10. *Invest. Radiol.* **39,** 56–63 (2004).
44. Fu, Y. S. *et al.* Stable aqueous dispersion of ZnO quantum dots with strong blue emission via simple solution route. *J. Am. Chem. Soc.* **129,** 16029–16033 (2007).
45. Sallusto, F., Cella, M., Danieli, C. & Lanzavecchia, A. Dendritic cells use macropinocytosis and the mannose receptor to concentrate macromolecules in the major histocompatibility complex class II compartment: downregulation by cytokines and bacterial products. *J. Exp. Med.* **182,** 389–400 (1995).

46. Long, C. M., van Laarhoven, H. W., Bulte, J. W. & Levitsky, H. I. Magnetovaccination as a novel method to assess and quantify dendritic cell tumor antigen capture and delivery to lymph nodes. *Cancer Res.* **69,** 3180–3187 (2009).
47. Saha, A. *et al.* Dendritic cells pulsed with an anti-idiotype antibody mimicking carcinoembryonic antigen (CEA) can reverse immunological tolerance to CEA and induce antitumor immunity in CEA transgenic mice. *Cancer Res.* **64,** 4995–5003 (2004).
48. Schneider, T. D. & Stephens, R. M. Sequence logos: a new way to display consensus sequences. *Nucleic Acids Res.* **18,** 6097–6100 (1990).

Acknowledgements

This work was supported by the Pioneer Research Center Program through the National Research Foundation of Korea funded by the Ministry of Education, Science and Technology (2011-0001715). Y.K.K. was supported by the Leap Research Program through the National Research Foundation of Korea (2011-0016497) and the Industrial Core Technology Development Program funded by the Ministry of Knowledge Economy (10033183). S.Y.S. and N.H.C. were supported by a grant from the Innovative Research Institute of Cell Therapy funded by the Ministry of Health and Welfare (A062260). T.C.C. and J.H.M. were supported by Hi Seoul Science/Humanities Fellowship from Seoul Scholarship Foundation. The authors are grateful to N. Orazio for critical reading of the manuscript.

Author contributions

N-H.C., S-Y.S. and Y.K.K. conceived and designed the experiments. T-C.C., J.H.M., J.H.W., S.J.L., D.H.K., J-S.Y. and S.K. performed the experiments. N-H.C., S-Y.S. and Y.K.K. analysed the data and wrote the paper. All authors discussed the results and commented on the manuscript.

Additional information

The authors declare no competing financial interests. Supplementary information accompanies this paper at www.nature.com/naturenanotechnology. Reprints and permission information is available online at http://www.nature.com/reprints. Correspondence and requests for materials should be addressed to Y.K.K. and S-Y.S.